2.4 VALIDATION OF TOP-OF-ATMOSPHERE LONGWAVE RADIATIVE FLUX ESTIMATES FROM CLOUDS AND THE EARTH'S RADIANT ENERGY SYSTEM (CERES) ANGULAR DISTRIBUTION MODELS

Konstantin Loukachine *
Science Applications International Corporation, Hampton, Virginia

Norman G. Loeb
Center for Atmospheric Sciences, Hampton University, Hampton, Virginia

Natividad Manalo-Smith
Analytical Services & Materials, Inc., Hampton, Virginia

1. INTRODUCTION

The conversion of the measured radiances to TOA radiative fluxes is an important step in estimating the planetary radiation budget from narrow field-of-view (FOV) satellite instruments. The emitted longwave radiation from a given region generally decreases with increasing viewing zenith angle, an effect known as limb-darkening. Therefore the conversion of the Earth's longwave radiance to flux requires the use of the angular distribution models (ADM). Development and validation of ADMs continues to be a major area of concern [*Smith et al., 1994*].

A unique combination of the multi-angule radiance measurements by CERES and high resolution imager data from the Visible Infrared Scanner (VIRS) on the Tropical Rainfall Measurement Mission (TRMM) was used to develop a new generation of CERES ADMs [*Loeb et al., 2002a; Manalo-Smith et al., 2002*]. The models are defined for several scene types and imager-based cloud properties [*Manalo-Smith et al., 2002*]. We emphasize that the simultaneous stratification of the scene type according to parameters, which are sensitive to the scene's anisotropy, is the major difference of CERES SSF ADMs from the previously applied to Earth Radiation Badget Experiment (ERBE) and TRMM measurements [*Suttles et al., 1988*].

In this study we compare the TOA longwave radiative fluxes based on the new CERES ADMs with the fluxes based on the ADMs developed for the ERBE.

2. VALIDATION RESULTS

To validate TOA longwave radiative fluxes we have used 8 months of the TRMM/CERES Single Scanner Footprint (SSF) data product with CERES in Rotaiting Azimuth Plane (RAP) scanning mode. By using RAP scanning mode over a period of time, the measurements cover a broad range of viewing zenith angle, and therefore allow a precise calculation of the directly integrated fluxes:

$$F_{DI} = 2\pi \int_0^{2/\pi} L(\theta)\, cos\theta\, sin\theta\, d\theta \ , \qquad (1)$$

which we consider as the "true" mean flux values. Ideally, the obtained TOA fluxes should have no dependence on viewing geometry, and should be close to the F_{DI}. For comparison we consider the ERBE-like CERES/TRMM product, obtained by application of ERBE algorithms to the same data sample [*Wielicki and Green, 1989*].

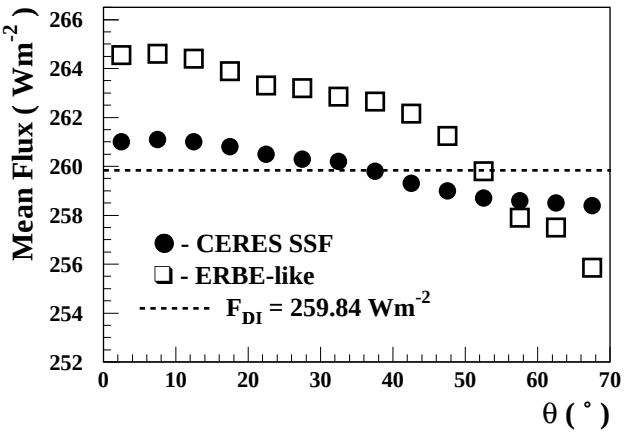

Figure 1: All-sky mean TOA LW flux stratified by viewing zenith angle, θ, for CERES SSF (filled circles) and ERBE-like (open squares) ADMs. The directly integrated flux, F_{DI}, is shown with a dashed line.

* *Corresponding author address:* K. Loukachine, SAIC, One Enterprise Parkway, Suite 300, Hampton, VA 23666; e-mail: k.loukachine@larc.nasa.gov

2.1 All-Sky

The all-sky TOA LW mean flux stratified by viewing zenith angle, θ, is shown in Fig. 1 for CERES SSF and ERBE ADMs. The value of the directly integrated flux over all viewing zenith angle is $F_{DI} = 259.84$ Wm^{-2} and is shown by a dashed line in Fig. Fig. 1. The remaining LW flux dependence on θ is greatly reduced for CERES SSF compared to ERBE ADMs. The difference of overall mean TOA flux and directly integrated flux is shown in Table 1.

	Mean Flux (Wm^{-2})	$F - F_{DI}$ (Wm^{-2})
CERES SSF	259.78	-0.06
ERBE-like	261.68	1.84

Table 1: TOA all-sky mean flux and difference between ADM and directly integrated fluxes.

The regional TOA LW flux bias for CERES SSF is also reduced factor of 4 compared with the ERBE-like fluxes [*Loeb et al., 2002b; Manalo-Smith et al., 2002*). The reduction in flux errors is due to better scene identification and further stratification of the ADMs in cloud parameters based on VIRS measurements.

2.2 Overcast Scenes

The CERES footprint size in the along-scan direction increases with viewing zenith angle, θ, from approximately 10 km at nadir to about 100 km at $\theta = 75°$. At full resolution, the overcast poplation at nadir is quite different from the overcast population at oblique viewing zenith angles. The latter likely contains a larger number of thick cold clouds since the clouds must be horizontally extensive (and likely more vertically developed) to be overcast at those spatial scales.
To avoid biases caused by the change in footprint size, we used reduced CERES resolution FOVs, built by averaging consecutive full resolution CERES footprints which cover distance in along-scan direction from 55 to 65 km (from trailing edge of the first included FOV to leading edge of the last FOV), 60 km in average. The fluxes and cloud parameters of the reduced resolution CERES FOV are obtained by averaging the values of the included full resolution footprints. Therefore we set an uniform spatial scale in defining the scene type. The 60 km distance was chosen to have a statistically significant sample of reduced resolution FOVs for all scene types, which

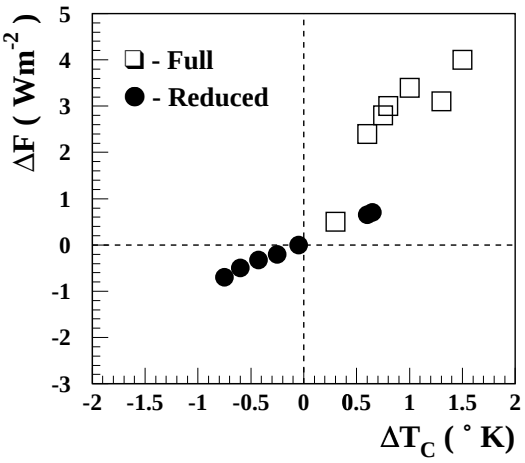

Figure 2: Average flux difference, ΔF, versus average cloud-top temperature difference, ΔT_C, for CERES full (open squares) and reduced (filled circles) resolution footprints for overcast cloud scenes.

cover a range up to 70° in CERES viewing zenith angle.
The difference in fluxes averaged for small and large viewing zenith angles,

$$\Delta F = F(\theta < 30°) - F(\theta > 40°),$$

plotted versus the differences in cloud-top temperature for small and large viewing zenith angles,

$$\Delta T_C = T_C(\theta < 30°) - T_c(\theta > 40°),$$

is shown in Fig. 2 for overcast cloud scenes. For full resolution CERES footprints, the ΔF and ΔT_C are both positive and strongly correlated. The remaining flux dependence on θ can be attributed to the dependence of cloud characteristics on the viewing geometry, as a consequence of different cloud population at different spatial scales. For the reduced resolution CERES FOV, the mean ΔF and ΔT_C are very close to zero. However, there is still a correlation between flux and cloud-top temperature biases.
Figure 3 shows the CERES SSF (black) and ERBE-like (transparent) ΔF distributions stratified by precipitable water (Fig. 3a) and cloud-top temperature (Fig. 3b) for reduced resolution overcast footprints. The ΔF should be equal to zero over entire variable range in the case of perfect flux inversion. The bias in ΔF is significantly reduced for CERES SSF compared with ERBE-like fluxes. The most noticeable improvement of about 5 Wm^{-2} is at typical cloud-top temperature $T_C \approx 250$ ° K.
The mean flux dependence on viewing zenith angle and the value of the directly integrated flux for

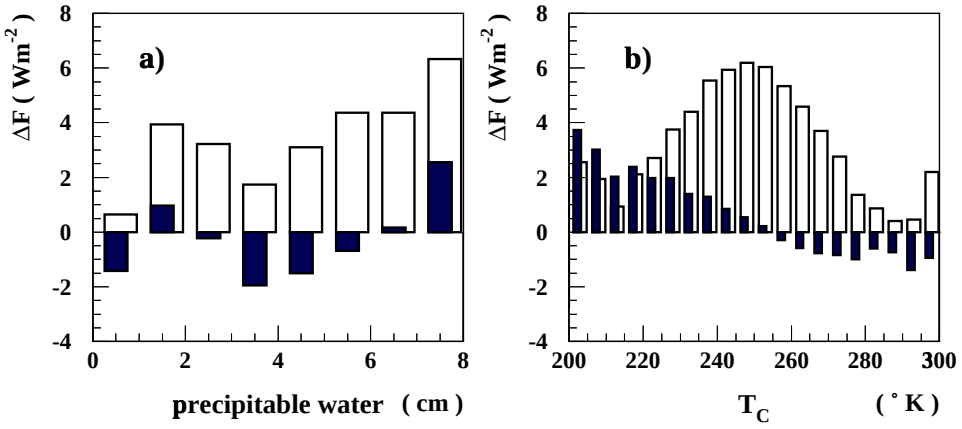

Figure 3: Overcast reduced resolution mean flux difference, ΔF, stratified by a) precipitable water, and (b) cloud-top temperature for the CERES SSF (black) and ERBE-like (transparent) ADMs.

overcast cloud layers is shown in Fig. 4 for CERES SSF (filled circles) and ERBE-like (open squares). The CERES SSF mean flux is remarkably close to the directly integrated flux. The ERBE-like mean flux is overestimated at small and underestimated at large viewing zenith angles.

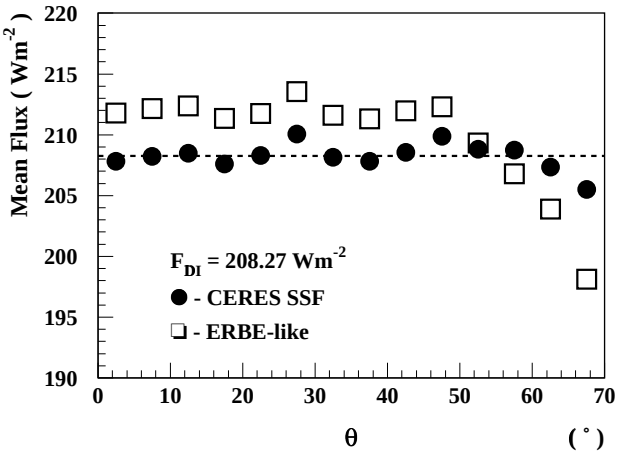

Figure 4: Overcast ADM mean flux for reduced resolution CERES FOVs stratified by CERES viewing zenith angle, θ, for CERES SSF (filled circles) and ERBE-like (open squares) ADMs. The dashed line shows the directly integrated flux value.

The difference between mean TOA flux and directly integrated flux for overcast scenes, $(F-F_{DI})$, is shown in Table 2.

	Mean Flux ($\mathrm{Wm^{-2}}$)	$F - F_{DI}$ ($\mathrm{Wm^{-2}}$)
CERES SSF	208.24	-0.03
ERBE-like	209.88	1.61

Table 2: TOA mean flux and difference between ADM and directly integrated fluxes for overcast cloud scenes.

3. SUMMARY AND CONCLUSIONS

The all-sky average regional longwave TOA flux bias for the CERES SSF is reduced by a factor of 4 compared to ERBE-like fluxes.

Spatial averaging of CERES FOVs removes the FOV size dependence on θ and eliminates apparent flux biases caused by changes in physical cloud properties with spatial resolution.

The CERES SSF LW fluxes show a much smaller dependence on θ than ERBE-like fluxes for all scene types.

REFERENCES

Smith, G.L., N. Manalo-Smith, L.M, Avis,1994: Limb-darkening Models from Along-Track Operation of the ERBE Scanning Radiometer, *J. Appl. Meteor.*, **33**, 74-84.

Suttles, J.T., *et al.*, 1988: Angular radiation models for Earth-atmosphere system, vol. II, in *Longwave Models, Rep. NASA RP-1184*, MASA, Washington, D.C.

Wielicki, B.A., and R.N. Green, 1989: Cloud identification for ERBE radiation flux retrieval, *J. Appl. Meteor.*, **28**, 1133-1146.

Wielicki, B.A., *et al.*, 1996: Clouds and the Earth's Radiant Energy System (CERES): An Earth observing system experiment, *Bull. Am. Meteor. Soc.*, **77**, 853-868.

Loeb, N.G., *et al.*, 2002a: Angular distribution models for top-of-atmosphere radiative flux estimation from the Clouds and the Earth's Radiant Energy System Instrument on the Tropical Rainfall Measuring Mission Satellite. Part I: Methodology, *J. Appl. Meteor.*, submitted.

Loeb, N.G., *et al.*, 2002b: A new generation of angular distribution models for top-of-atmosphere radiative flux estimation from the Clouds and the Earth's Radiant Energy System (CERES) satellite instrument. *11th Conference on Atmospheric Radiation, proceedings*, Paper 2.3.

Manalo-Smith, N., N.G. Loeb, K. Loukachine, 2002: Development of longwave and window angular distribution models from the Clouds and Earth's Radiant Energy System (CERES) experiment. *11th Conference on Atmospheric Radiation, Proceedings*, Paper P2.4.